# Disruption of the cingulin gene does not prevent tight junction formation but alters gene expression

**Laurent Guillemot[1], Eva Hammar[1], Christian Kaister[1], Jorge Ritz[1,2], Dorothée Caille[3], Lionel Jond[1], Christoph Bauer[1,2], Paolo Meda[3] and Sandra Citi[1,4,*]**

[1]Department of Molecular Biology, University of Geneva, 30 Quai Ernest-Ansermet, 1211 Genève 4, Switzerland
[2]NCCR 'Frontiers in Genetics', University of Geneva, 30 Quai Ernest-Ansermet, 1211 Genève 4, Switzerland
[3]Department of Cell Physiology and Metabolism, CMU, University of Geneva, 1 Rue Michel Servet, 1211 Genève 4, Switzerland
[4]Department of Biology, University of Padova, Via U. Bassi 58B, 35121 Padova, Italy
*Author for correspondence (e-mail: sandra.citi@molbio.unige.ch)

*Accepted 6 July 2004*
*Journal of Cell Science 117, 5245-5256 Published by The Company of Biologists 2004*
*doi:10.1242/jcs.01399*

## Summary

**Cingulin, a component of vertebrate tight junctions, contains a head domain that controls its junctional recruitment and protein interactions. To determine whether lack of junctional cingulin affects tight-junction organization and function, we examined the phenotype of embryoid bodies derived from embryonic stem cells carrying one or two alleles of cingulin with a targeted deletion of the exon coding for most of the predicted head domain. In homozygous (–/–) embryoid bodies, no full-length cingulin was detected by immunoblotting and no junctional labeling was detected by immunofluorescence. In hetero- and homozygous (+/– and –/–) embryoid bodies, immunoblotting revealed a Triton-soluble, truncated form of cingulin, increased levels of the tight junction proteins ZO-2, occludin, claudin-6 and Lfc, and decreased levels of ZO-1. The +/– and –/– embryoid bodies contained epithelial cells with normal tight junctions, as determined by freeze-fracture and transmission electron microscopy, and a biotin permeability assay. The localization of ZO-1, occludin and claudin-6 appeared normal in mutant epithelial cells, indicating that cingulin is not required for their junctional recruitment. Real-time quantitative reverse-transcription PCR (real-time qRT-PCR) showed that differentiation of embryonic stem cells into embryoid bodies was associated with up-regulation of mRNAs for several tight junction proteins. Microarray analysis and real-time qRT-PCR showed that cingulin mutation caused a further increase in the transcript levels of occludin, claudin-2, claudin-6 and claudin-7, which were probably due to an increase in expression of GATA-6, GATA-4 and HNF-4α, transcription factors implicated in endodermal differentiation. Thus, lack of junctional cingulin does not prevent tight-junction formation, but gene expression and tight junction protein levels are altered by the cingulin mutation.**

Supplementary material available online at
http://jcs.biologists.org/cgi/content/full/117/22/5245/DC1

Key words: Cingulin, Tight junction, Epithelium, Differentiation, Embryoid body, ES cell

## Introduction

In vertebrate epithelial cells, tight junctions (TJs) form a circumferential apical belt that acts as a barrier that controls paracellular permeability across epithelial sheets and a fence that maintains plasma-membrane polarity. TJs contain several types of transmembrane molecule, including tetraspan membrane proteins and Ig-like adhesion molecules, which mediate cell-cell adhesion and constitute the paracellular channels through which ions, water, molecules and cells permeate epithelial sheets. The cytoplasmic face of TJs consists of a complex network of proteins, including PDZ-domain-containing proteins, evolutionarily conserved polarity determinants, cytoskeletal adaptors, small GTP-binding proteins, protein kinases and phosphatases (for reviews, see Citi, 2001; D'Atri and Citi, 2002; Gonzalez-Mariscal et al., 2003; Tsukita et al., 2001). In addition, the recent identification of transcription factors as TJ components (Balda and Matter, 2000; Betanzos et al., 2004; Nakamura et al., 2000) points to TJs as platforms that integrate signals between neighboring cells and the nucleus to coordinate cell growth and differentiation (Matter and Balda, 2003).

The clarification of the molecular organization of TJs should provide a rational basis for understanding how these junctions carry out their diverse functions. Some genetic evidence for a role of junctional proteins in TJ organization and epithelial function in vertebrates has recently emerged. With regard to integral membrane components of TJs, we know that targeted deletion of occludin in mouse embryonic stem (ES) cells results in embryoid bodies (EBs) with morphologically and functionally normal TJs (Saitou et al., 1998), and occludin deletion resulted in viable mice with a complex pathological phenotype (Saitou et al., 2000). Mutations of claudin-11 (Gow et al., 1999), claudin-16/paracellin-1 (Hirano et al., 2000; Simon et al., 1999), claudin-14 (Ben-Yosef et al., 2003; Wilcox et al., 2001) and claudin-5 (Nitta et al., 2003) result in pathological phenotypes that appear to be confined to the tissues in which these isoforms are expressed. Claudin-1-knockout mice display an early postnatal lethal phenotype, owing to transepidermal water loss (Furuse et al., 2002). By contrast, genetic evidence for a role of the cytoplasmic protein components of vertebrate TJs is limited. Deletion of AF-6/afadin, a protein believed to be associated with both TJs and

adherens-type junctions, leads to an early embryonic lethal mouse phenotype, with loss of neuroepithelial polarity (Ikeda et al., 1999; Zhadanov et al., 1999). Nothing is known about the consequences of a genetically targeted mutation of any other TJ cytoplasmic component.

Cingulin is a 140-160-kDa protein component of the cytoplasmic plaque of vertebrate TJs that was originally identified as an actomyosin-associated protein (Citi et al., 1988). Cingulin might play an important role in the biology of vertebrate epithelia, because it is one of the first proteins that assembles into TJs in early vertebrate embryos (Cardellini et al., 1996; Fesenko et al., 2000; Fleming et al., 1993). The cingulin sequence predicts that the molecule is a parallel homodimer, made by two subunits that consist of a central coiled-coil rod domain that separates a large, globular N-terminal head domain and a small, globular C-terminal tail (Cordenonsi et al., 1999a). The head domain controls junctional recruitment and mediates direct in vitro interaction with the TJ proteins ZO-1, ZO-2, JAM-1 and actin, through sequences located in its N-terminal half (Bazzoni et al., 2000; Cordenonsi et al., 1999a; D'Atri and Citi, 2001; D'Atri et al., 2002). The rod domain mediates dimerization, interaction with myosin and possibly intramolecular interaction (Citi et al., 2000; Cordenonsi et al., 1999a). In vivo, cingulin forms a complex with ZO-1, ZO-2 (Cordenonsi et al., 1999a) and JAM-1 (Bazzoni et al., 2000), suggesting that it might functionally link TJ proteins to the actomyosin cytoskeleton during TJ biogenesis and regulation.

Here, we report a genetic approach to dissect the role of cingulin at TJs. Because the head domain is crucial for the junctional localization and protein interactions of cingulin, we constructed targeting vectors designed to delete the exon that codes for most of the putative head region sequence, in mouse ES cells, resulting in TJs that lack cingulin. Characterization of EBs obtained from wild-type (+/+), heterozygous (+/–) and homozygous mutant (–/–) ES cells shows that cingulin mutation did not perturb the formation of TJs but altered the expression of certain TJ proteins and transcription factors.

## Materials and Methods

### Antibodies

Antibodies against the following proteins were used. Cingulin: Zymed 36-4401, C532 (Cardellini et al., 1996), Zymed 37-4300. ZO-1: Zymed 61-7300, R40-76 (B. Stevenson, Salk Institute, USA) (Stevenson et al., 1986). ZO-2: Zymed 71-1400, Santa Cruz Biotechnology H-110. ZO-3: Santa Cruz Biotechnology H-130. Occludin: Zymed 71-1500. Claudin-6: (S. Tsukita and M. Furuse, Kyoto University, Japan). JAM-1: (D. Vestweber, University of Münster, Münster, Germany) (Ebnet et al., 2000). PAR-3: Zymed 36-2301. Lfc and Ybx3 (ZONAB): B4/7 and YB3 (K. Matter and M. Balda, University College London, London, UK) (Balda and Matter, 2000; Benais-Pont et al., 2003). α-Tubulin: (T. Kreis, University of Geneva, Switzerland). Horseradish-peroxidase (HRP)-labeled antibodies for immunoblotting (ECL) were from Promega. Fluorescein isothiocyanate (FITC)- and Cy5-labeled antibodies for immunofluorescence were from Jackson Immunoresearch Laboratories.

### Cell culture and EB formation

Mouse ES cells (clone D3) were cultured on embryonic feeder cells in Dulbecco's modified Eagle's medium (Sigma) containing 15% fetal bovine serum (FBS), 4 mM L-glutamine, 1 mM sodium pyruvate, 1× MEM non-essential amino acids, 50 μg $ml^{-1}$ gentamycin, 0.1 mM 2-mercaptoethanol and 1000 U $ml^{-1}$ leukemia inhibitor factor (LIF). Every 2-3 days, the cultures were passaged (1:10). For cystic EB formation, $0.7\times10^6$ ES cells were cultured on gelatin-coated 10-cm culture dishes for 3 days in normal LIF-containing medium. $2\times10^6$ cells were then inoculated into a 10-cm non-tissue-culture-treated dish, preventing cell attachment. EBs were grown in suspension culture for 10 days in the absence of LIF. To control for possible clone-related differences in phenotype, two independent clones of wild-type (WT1 and WT2), heterozygous (+/–) (1;166 and 1;10), and homozygous (–/–) (3;4 and 3;96) cells were used in each experiment. The six clones were cultured in parallel and were of similar passage number, to minimize the influence of culture conditions and passage number on the results.

### Gene targeting

Fragments of the genomic locus encoding mouse cingulin were isolated from a phage of a λFixII 129/Sv mouse genomic library (J. Ripperger, University of Geneva, Switzerland), screened with a fragment of human cDNA encoding the cingulin head, and by restriction digestion from a RPCI23 bacterial artificial chromosome clone (4p7). The putative exon organization of the mouse cingulin-encoding gene (chromosome 3) is available at http://www.ncbi.nlm.nih.gov/sutils/evv.cgi?contig=NT_080250&gene=Cgn&lid=70737&taxid=10090. By analogy with the organization of the human cingulin-encoding gene and cDNA sequence, we hypothesize that the putative exon 2 identified in the genomic fragment corresponds to the first coding exon. To construct the first targeting vector, a neomycin-resistance (Neo) cassette (1.9 kb) was isolated by *Kpn*I-*Xba*I digestion of plasmid pHR-68 (F. Spitz, University of Geneva, Switzerland) and was ligated with a 2.4 kb *Xba*I-*Eco*RV fragment of the cingulin-encoding gene (right arm, downstream of exon 2) into plasmid pKS+, which was cut with *Kpn*I and *Eco*RV. The Neo cassette and right arm were excised from this construct by digestion with *Kpn*I and *Not*I, and ligated with a 5.5 kb *Xho*I-*Kpn*I fragment (left arm, upstream of exon 2) into pKS+, which was cut with *Xho*I and *Not*I, to obtain the Neo targeting vector. A second targeting vector was constructed using the same strategy, except that a hygromycin resistance cassette (2.2 kb) was isolated by digestion of plasmid pSK-Hygro (F. Spitz). The targeting vectors were linearized by *Not*I digestion and 10 μg DNA was used to electroporate ES cells ($10^7$), using a Gene Pulser (BioRad) at 400 V, 125 μF for 2-2.5 milliseconds. After 48 hours, cells were selected in antibiotic-containing medium (200 μg $ml^{-1}$ neomycin and/or 150 μg $ml^{-1}$ hygromycin) for 7 days. Antibiotic-resistant colonies were collected, expanded into 48-well plates, duplicated and inoculated into 24-well gelatin-coated plates. When confluent, cells were rinsed with PBS (10 mM $Na_2HPO_4$, 1.7 mM $KH_2PO_4$, 136 mM NaCl, 2.6 mM KCl, pH 7.4) and lysed in 0.5 ml lysis buffer [50 mM Tris-HCl, pH 8.0, 100 mM NaCl, 10 mM EDTA, 0.5% sodium dodecyl sulfate (SDS), 100 μg $ml^{-1}$ proteinase K] for 24 hours at 37°C.

### Genomic Southern blot analysis

For DNA isolation, lysates were extracted in 0.2 M NaCl and phenol (1:1 phenol/chloroform:aqueous phase). Genomic DNA samples were digested with either *Apa*I (16 hours, 25°C) or *Eco*RI (16 hours, 37°C), electrophoresed on 0.65% agarose gels and transferred to positively charged nylon membranes (Roche). Blots were hybridized with digoxygenin (DIG)-labeled probes generated by PCR. The 3′ probe (727 bp) was obtained using the primers 5′-AGATTTCTCTCCCATA-CATATATAT-3′ and 5′-ATTATTGCAGGCTTGGCAGGG-3′, and was used for analysis of *Apa*I genomic digests. The 5′ probe was obtained using the primers 5′-AGAAAATGAAGATCTCGGCTCTG-3′ and 5′-CTCGAGCATACTCCTGAGGAC-3′ followed by digestion with *Sac*II. The resulting 294 bp fragment was used for analysis of *Eco*RI genomic digests. Targeted clones were also checked for single

integration by hybridization with either an 803 bp neo probe or a 310 bp hygro probe (Fig. 1).

### Preparation of cell lysates

EBs were washed twice with PBS containing 1 mM $CaCl_2$ and 0.5 mM $MgCl_2$, and lysed for 15 minutes with ice-cold lysis buffer (150 mM NaCl, 50 mM Tris-HCl, pH 7.4, 1% Triton X-100, 5 μg $ml^{-1}$ antipain, 5 μg $ml^{-1}$ leupeptin, 5 μg $ml^{-1}$ pepstatin, 0.1 mM phenylmethylsulfonyl fluoride). Lysates were centrifuged at 13,000 ***g*** for 15 minutes at 4°C and the supernatant (Triton-soluble fraction) was collected. The pellet was resuspended and incubated for 15 minutes in lysis buffer containing 1% SDS. Following centrifugation, the supernatant (Triton-insoluble fraction) was collected.

### Immunoblotting

SDS polyacrylamide-gel electrophoresis (SDS-PAGE) gels were transferred to nitrocellulose membranes by semi-dry blotting and processed as previously described (D'Atri et al., 2002), except that secondary antibodies were HRP coupled. Protein loadings were normalized using as internal standard endogenous α-tubulin. Immunoblots were developed by an enhanced chemiluminescence kit (Pierce). Autoradiograms were scanned and analysed with the BioRad QuantityOne software.

### cRNA preparation and microarray analysis

Total RNA was isolated from cytoplasm of three independent preparations of EBs from wild-type (WT1) and cingulin homozygous (–/–) (3;4) clones, using the RNeasy mini kit (Qiagen). Reverse transcription was performed on 15 μg total RNA for 1 hour at 42°C using a T7-oligo (dT)24-primer and Superscript II Reverse Transcriptase (Gibco). Second-strand cDNA synthesis was for 2 hours at 16°C using *Escherichia coli* DNA polymerase I, DNA ligase and RNase H (Gibco), followed by incubation with T4 DNA Polymerase (Gibco) for 5 minutes at 65°C. After phenol/chloroform extraction, in vitro transcription was performed for 4 hours at 37°C, using Bio-16-UTP, Bio-11-CTP and T7 RNA Polymerase (Enzo, New York, NY). cRNA was purified using RNeasy (Qiagen) followed by fragmentation for 35 minutes at 95°C. For RNA quality control, 4.5 μg labeled cRNA were run on Test3 arrays (Affymetrix). The Affymetrix Mouse 430A expression arrays (contains probe sets against 14,484 well-annotated full-length genes, 4371 expressed sequence tag sequences and 3771 non-expressed-sequence-tag sequences) were hybridized with 12 μg labeled cRNA for 16 hours at 45°C under rotation and stained in an Affymetrix Fluidics station with streptavidin-phycoerythrin, followed by staining with a biotinylated anti-streptavidin antibody and streptavidin-phycoerythrin. The arrays (three per sample) were scanned with a GeneCHIP scanner, and data were analysed with the Affymetrix statistics-based software MAS-5.0. Fold changes were calculated by dividing the expression level of each individual gene in cingulin homozygous (–/–) EBs (3;4) by the expression level of the same gene in wild-type EBs (WT1). A significant change was defined as a fold increase or decrease that had the same value in the nine comparisons obtained from three microarrays of wild-type EBs and three microarrays of cingulin homozygous (–/–) EBs, and when the *P* value was below 0.05 (in a Student's *t* test). Data are presented as means from the nine cross comparisons.

### Real-time quantitative reverse-transcription PCR

For real-time quantitative reverse-transcription PCR (real-time qRT-PCR), total RNA was prepared from three independent cultures of each of the six ES cell clones and EBs using the RNeasy mini kit (Qiagen). cDNA synthesis was achieved with 1-2 μg of total RNA using the iScript cDNA synthesis kit (BioRad). SYBR-Green-based real-time PCR was used to measure relative gene expression in each sample. Each master mix (25 μl) contained a single gene-specific primer set (forward and reverse, 2.5 μM) (Table 1), 20 ng of cDNA, 10 nM fluorescein calibration dye and 2×-SYBR-Green PCR mastermix (Applied Biosystems). Assays were carried out using 96-well plates. Each experimental sample was assayed using three replicates for each primer, including the *HPRT*-specific primer that was used as an internal standard. Negative controls lacking the cDNA template were run with every assay to assess specificity. Gene-specific primer sets were designed using PrimerExpress sofware (Applied Biosystems) and are listed in Table 1. Full-length cingulin expression was analysed with primers within the head region. *ZO-1* mRNA was amplified with primers within or outside the α domain, to analyse separately the expression of ZO-1$\alpha^+$ and ZO-1$\alpha^-$, two isoforms that are expressed differently during mouse development and in adult tissues (Balda and Anderson, 1993; Sheth et al., 1997; Willott et al., 1992). The real-time fluorescence signal was analysed using the

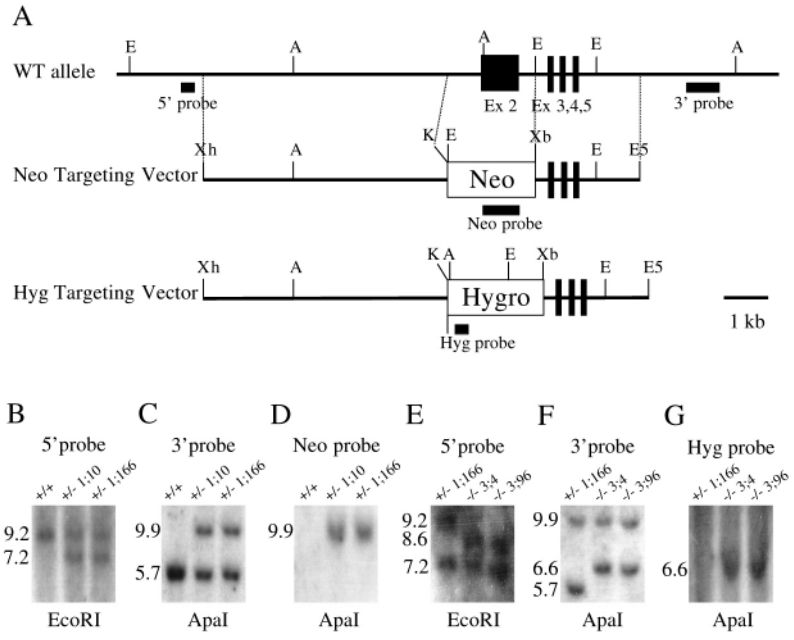


**Fig. 1.** Targeting of cingulin alleles by homologous recombination in mouse ES cells. (A) Restriction maps of the cingulin genomic locus [wild-type (WT) allele] and the neomycin (Neo) and hygromycin (Hyg) targeting vectors. Putative exons 2-5 are represented by black boxes. A 1.98 kb *Kpn*I-*Xba*I fragment beginning 775 bp upstream of the ATG translation start codon and ending 353 bp downstream of the 3′ end of exon 2 was replaced by a neomycin-resistance cassette in the first targeted allele and by a hygromycin resistance cassette in the second targeted allele. In the targeting vectors, the antibiotic resistance cassettes were flanked on the 5′ side by a 5.5 kb *Xho*I-*Kpn*I intron fragment (left arm) and on the 3′ side by a 2.4 kb *Xba*I-*Eco*RV fragment (right arm) containing intronic sequences and exons 3-5. Positions of the 5′ and 3′ probes, and the neomycin and hygromycin probes used for Southern-blot analyses are shown as thick lines. A, *Apa*I; E, *Eco*RI; E5, *Eco*RV; K, *Kpn*I; Xb, *Xba*I; Xh, *Xho*I. (B-G) Southern-blot analysis. Restriction endonucleases used for digestions are indicated beneath each blot. Genotypes and probes are indicated above each blot. Sizes (kb) of hybridizing bands are indicated on the left.

**Table 1. Sequences of primers used in real-time qRT-PCR**

| Gene | Forward primer | Reverse primer |
|---|---|---|
| Cingulin | 5′-CTAAACCGACTTCCTCGATTAA-3′ | 5′-TGTTGATGAGCGAGTCCACTG-3′ |
| ZO-1 $\alpha^-$ | 5′-CCCTACCAACCTCGGCCTT-3′ | 5′-AACGCTGGAAATAACCTCGTTC-3′ |
| ZO-1 $\alpha^+$ | 5′-CGCCAAATGCGGTTGATC-3′ | 5′-TTTACACCTTGCTTAGAGTCAGGGTT-3′ |
| ZO-2 | 5′-AGCACGCCCTGCTCGAC-3′ | 5′-TCACGATTGGAAACCACTGAGT-3′ |
| ZO-3 | 5′-ACCCTATGGCCTGGGCTTC-3′ | 5′-CCCGGGTACAACGTGTCC-3′ |
| Claudin-2 | 5′-CCCAGGCCATGATGGTGA-3′ | 5′-TCATGCCCACCACAGAGATAAT-3′ |
| Claudin-6 | 5′-ATGTGGAAGGTGACCGCCT-3′ | 5′-CCCTCCCACACCATCTGG-3′ |
| Claudin-7 | 5′-CCTGGTGTTGGGCTTCTTAGC-3′ | 5′-CCCACAGCGTGTGCACTTC-3′ |
| Occludin | 5′-CCAGGCAGCGTGTTCCT-3′ | 5′-TTCTAAATAACAGTCACCTGAGGGC-3′ |
| JAM-1 | 5′-AGCTCCCTATGCGGACCG-3′ | 5′-CCTTCCGGGTCACAGAACTG-3′ |
| PAR-3 | 5′-TTCCGCCAAGCTATGCGT-3′ | 5′-CATATTGCTCCTTGTTTGCTGC-3′ |
| Lfc | 5′-TCACGCTGGATTATGTCTCGG-3′ | 5′-CCTGCTCCTTGCTCCGGT-3′ |
| Ybx3 | 5′-CGCCGTTCCCGTCCC-3′ | 5′-TGGTGCTTCACCTGCCTTG-3′ |
| HPRT | 5′-TTTGCCGCGAGCCG-3′ | 5′-TAACCTGGTTCATCATCGCTAATC-3′ |

iCycler iQ software v3.0 (BioRad). The cycling conditions were: one cycle at 95°C for 10 minutes, followed by 40 cycles of PCR amplification, each consisting of 95°C for 15 seconds and 60°C for 45 seconds. To identify specific PCR products, melting-curve analysis was performed by heating the reaction mixture from 60°C to 95°C at a rate of 0.5°C per 10 seconds. A threshold cycle (C*t*) was determined for each sample using the exponential-growth phase and the baseline signal from fluorescence versus cycle number plots. PCR assays that showed non-specific products at the end point were excluded from further data analysis. Δ*Ct* values were obtained by subtracting the C*t* value of the housekeeping gene *HPRT* from the C*t* value for each indicated gene. Each Δ*Ct* value represents the means±S.D. of three independent experiments. Δ*Ct* values are shown in Supplementary Table 1 (see Table S1 in supplementary material). Δ*Ct* averages for each gene were calculated from Δ*Ct* values evaluated in the two clones of the same genotype. ΔΔ*Ct* were calculated as the differences in Δ*Ct* averages between wild-type (+/+), heterozygous (–/+) and homozygous (–/–) EB and ES cells. Positive ΔΔ*Ct* values indicate more PCR cycles and therefore less mRNA. Conversely, negative ΔΔ*Ct* values indicate more mRNA. The fold change was calculated by $2^{-(\Delta\Delta Ct)}$. No change (NC) was scored when $P>0.05$. Student's *t* test was performed using the GraphPad Prism software.

### Immunofluorescence and confocal microscopy

EBs were fixed with 4% paraformaldehyde in 0.1 M sodium phosphate, pH 7.4, equilibrated with 30% sucrose, embedded in Tissue-Tek (Sakura, The Netherlands) and frozen in liquid nitrogen. 10 μm cryostat sections were dried onto SuperFrost Plus slides, fixed in ethanol at 4°C for 30 minutes, followed by acetone at room temperature for 1 minute. Incubations with primary and secondary antibodies were for 45 minutes at 37°C. 1 μm optical sections were imaged using a confocal fluorescence microscope (Zeiss LSM-510 Meta) equipped with a 63× (1.3 NA) objective.

### Ultrathin-section electron microscopy

EBs were fixed with 3% glutaraldehyde in 0.1 M sodium cacodylate buffer, pH 7.2, containing 2 mM $CaCl_2$ and postfixed with 1% $OsO_4$, 0.8% $K_3Fe(CN)_6$ in the same buffer. Samples were embedded in Type-VII agarose, stained en bloc with 4% uranyl acetate, dehydrated with a graded ethanol series and 100% propylene oxide, and embedded in Epoxy medium (Fluka). Ultrathin sections (70 nm) were stained with saturated uranyl acetate and 2.5% lead citrate, and examined using a Philips EM410 electron microscope. Measurements were carried out on photographs (12-16 per sample) of lateral membranes cut perpendicular to the apical surface of cells. TJ thickness was defined as the distance between the most apical and basal focal membrane interconnections.

### Freeze-fracture electron microscopy

EBs were fixed for 60 minutes in 2.5% glutaraldehyde solution in 0.1 M phosphate buffer, pH 7.4, infiltrated with 30% glycerol, frozen in Freon22 cooled in liquid nitrogen and processed for freeze-fracture using a BAF300 machine (Balzers High Vacuum, Balzers, Liechtenstein). Specimens were examined with a Philips CM10 electron microscope and photographs were taken at the magnification of 39,000×. Quantitative analysis of the number of strands (the thread-like mostly straight and parallel arrangements of TJ fibrils) per TJ belt and of the length of TJ fibrils (the linear organization of particulate transmembrane proteins running between two other similar structures) was carried out using a ACECAD Professional graphic tablet connected to a Quantimet Leica 500+ system (Leica, Cambridge, UK). Statistical comparisons were carried out by analysis of variance and median tests, as provided by the Statistical Package for Social Sciences (SPSS, Chicago).

### TJ permeability assay

The barrier function of epithelial cells of cystic EBs was studied using the surface biotinylation technique (Chen et al., 1997) with modifications (Saitou et al., 1998). Cryostat sections were labeled with fluorescein-conjugated avidin (Pierce) and TRITC-phalloidin (Sigma) to visualize surface biotin and actin filaments, respectively.

## Results

### Disruption of the cingulin-encoding gene by homologous recombination

DNA corresponding to the cingulin-encoding locus was isolated from a mouse genomic DNA library and used for construction of targeting vectors. Several putative exons were identified within a ~17 kb genomic DNA fragment (Fig. 1A). We denoted exon 2 an 852 bp exon containing sequence corresponding to the putative N-terminal region (residues 1-284) of mouse cingulin. In human and *Xenopus* cingulin, the sequences contained within this region are crucial for the junctional recruitment of cingulin and its interactions with ZO-1 and other proteins (D'Atri et al., 2002). Thus, targeted deletion of this exon is expected to eliminate cingulin localization to junctions. Two targeting vectors were designed to replace exon 2 and adjacent sequences (775 bp upstream of the ATG start codon and 353 bp downstream of the 3′ splice site) with either a neomycin or a hygromycin antibiotic-resistance cassette (Fig. 1A).

Wild-type (+/+) ES cells were transfected with the neomycin

targeting vector, and 192 neomycin-resistant clones were isolated. Southern-blot analysis of genomic DNA with probes in the 5′ and 3′ flanking regions and the Neo cassette showed that a homologous recombination event had occurred in four clones, as judged by the generation of restriction fragments of the expected size [Fig. 1B-D shows two of these (+/–) clones]. To target the remaining wild-type cingulin allele, one of the heterozygous (+/–) ES clones (1;166) was transfected with the hygromycin targeting vector. After selection, 192 clones were picked, and two homozygous mutant (–/–) clones were isolated (3;4 and 3;96), as shown by Southern-blot analysis with 5′, 3′ and hygromycin probes (Fig. 1E-G).

To study the effects of the cingulin mutation on the structure and function of TJs, ES cells were induced to differentiate into EBs under suspension culture conditions. After 10 days, cystic EBs were obtained, which contained a cavity filled with secreted fluid and an outer epithelial layer of visceral endoderm (Fig. 3). Two independent wild-type clones (WT1 and WT2), two independent heterozygous (+/–) clones (1;10 and 1;166) and both homozygous (–/–) clones (3;4 and 3;96) were used for subsequent experiments, to control for possible clonal differences that might be independent of the cingulin mutation.

## Cingulin mutation is associated with changes in the protein levels of ZO-1, ZO-2, claudin-6, occludin and Lfc in EB lysates

Cingulin interacts with several TJ proteins, so we tested whether the disruption of the cingulin-encoding gene affected the expression level of TJ proteins. EB lysates were fractionated into Triton-soluble (cytoplasmic) and Triton-insoluble (membrane/cytoskeleton-associated) pools, and were analyzed by immunoblotting with antibodies against major membrane and cytoplasmic TJ components (Fig. 2).

The ~140 kDa full-length cingulin polypeptide was detected at similar levels in both Triton-soluble and Triton-insoluble fractions of (+/+) and (+/–) EBs, but not in (–/–) EBs (Fig. 2, FL). However, anti-cingulin antibodies (which cross-react with the rod domain) labeled a ~100 kDa polypeptide in lysates of (+/–) and (–/–) EBs (Fig. 2, T). This truncated protein was detected exclusively in the Triton-soluble fraction, indicating that it is not part of the cytoskeletal complex underlying the TJ membrane. In addition, the cingulin rod sequence was detected by real-time qRT-PCR in heterozygous and homozygous mutant EBs (data not shown). This is consistent with aberrant initiation of translation downstream of exon 2 in targeted clones, resulting in the expression of a truncated cingulin. We observed a marked decrease in the levels of ZO-1 (Stevenson et al., 1986) in both Triton-soluble and Triton-insoluble fractions of heterozygous (+/–) and homozygous (–/–) EBs (Fig. 2). In addition, the levels of ZO-2 (Gumbiner et al., 1991) were slightly increased in the Triton-insoluble fraction of heterozygous (+/–) and homozygous (–/–) EBs (Fig. 2). By contrast, the levels of ZO-3 (Haskins et al., 1998), JAM-1 (Martin-Padura et al., 1998), PAR-3 (Izumi et al., 1998) and the Y-box-protein 3 [Ybx3; a mouse homolog of the canine TJ component ZONAB (Balda and Matter, 2000)], were very similar in both Triton-soluble and Triton-insoluble fractions of (+/+), (+/–) and (–/–) EBs

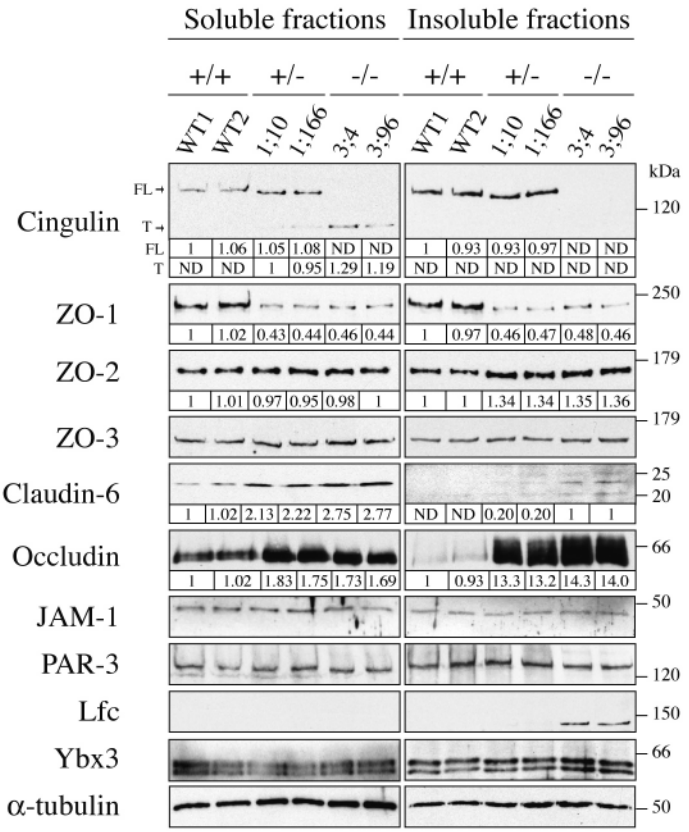


**Fig. 2.** Levels of ZO-1, ZO-2, claudin-6, occludin and Lfc proteins are altered following cingulin mutation in EBs. Triton-soluble and Triton-insoluble fractions of wild-type (+/+), heterozygous (+/–) and homozygous (–/–) EBs (genotype and clone name indicated above each lane) were analysed by SDS-PAGE and western blotting using antibodies against the proteins indicated on the left. Anti-α-tubulin signal was used to normalize protein loading. Numbers on the right indicate size (kDa) of protein markers. FL, full-length cingulin (~140 kDa); T, truncated cingulin (~100 kDa). Densitometric analysis was performed to measure protein levels when marked differences were observed. The numbers below the cingulin, ZO-1, ZO-2, claudin-6 and occludin lanes represent the signal intensity (mean of at least three independent experiments, one of which is shown here) relative to an arbitrary level of 1, corresponding to a reference lane for each set. ND, not detected.

(Fig. 2). Levels of claudin-6 (Morita et al., 1999) were increased in the Triton-soluble fraction of both heterozygous (+/–) and homozygous (–/–) EBs (Fig. 2). Claudin-6 was also detectable, although at low levels, in the Triton-insoluble fraction of the heterozygous (+/–) and homozygous (–/–) EBs (Fig. 2). Occludin levels were also increased in heterozygous (+/–) and homozygous (–/–) EBs in the Triton-soluble and, particularly, the Triton-insoluble fraction (Fig. 2). The Rho-specific exchange factor Lfc, whose canine homolog is a component of TJs (Benais-Pont et al., 2003), was detectable only in the Triton-insoluble fraction of (–/–) EB lysates (Fig. 2).

## Cingulin-mutant EBs show increased levels of mRNAs encoding claudin-2, claudin-6, claudin-7 and occludin

Cingulin mutation resulted in changes in the levels of ZO-1,

ZO-2, claudin-6, occludin and Lfc, so we next asked whether these altered protein levels were a consequence of altered mRNA levels. First, we compared EBs derived from wild-type (WT1) and homozygous (–/–) (3;4) ES cells by microarray analysis, which allowed us to examine mRNA levels for most TJ proteins. No significant change in mRNA levels was detectable for ZO-1, ZO-2, ZO-3, JAM-1, PAR-3 or Lfc (Table 2). However, (–/–) EBs showed a significant increase in mRNA levels for claudin-2 (~21-fold), claudin-6 (~2.4-fold), claudin-7 (~3-fold) and occludin (~2.8-fold) (Table 2). No change was detected for claudins 1 to 19 (NB claudin-12, claudin-17, cingulin and Ybx3 were not included in the microarray; data not shown).

Second, to explore mRNA expression levels using a more quantitative method, two independent clones per genotype were analysed by real-time qRT-PCR (Table 3). We focused on the genes that showed variation by microarray analysis and for which we had immunoblot data. RNA was prepared from both ES cells and EBs in order to determine whether gene expression changed with differentiation. For each gene, Δ*Ct* values were determined, corresponding to mRNA levels that were normalized to the housekeeping gene *HPRT*. In each set of samples, the Δ*Ct* values of the two clones of each genotype were similar (see Table S1 in supplementary material), indicating that differences between (+/+) and (–/–), and those between (+/+) and (+/–) cells were not due to a clonal variation. Δ*Ct* averages could then be calculated between clones of each genotype, followed by determination of ΔΔ*Ct* values. This allowed us to calculate the fold change in mRNA levels between the different genotypes (Table 3).

When comparing wild-type and mutant ES cells, the only significant difference in mRNA levels was detected for cingulin (Table 3A). In (+/–) ES cells, there was a ~1.9-fold decrease in the message levels of full-length cingulin. In (–/–) ES cells, there was no detectable cingulin message, consistent with the expected loss of expression of the wild-type cingulin molecule. When comparing wild-type and mutant EBs, mRNA coding for full-length cingulin was undetectable in (–/–) EBs, whereas, in heterozygous (+/–) EBs, cingulin-encoding mRNA levels were similar to wild-type EBs (Table 3B). Furthermore, both (+/–) and (–/–) EBs featured increased mRNA levels of claudin-2 [~15.3-fold in (+/–) and ~19.4-fold in (–/–)], claudin-6 [~2.5-fold in (+/–) and ~2.3-fold in (–/–)], claudin-7 [~3.9-fold in (+/–) and ~3.7-fold in (–/–)] and occludin [~3.1-fold in (+/–) and ~2.9-fold in (–/–)] (Table 3B). By contrast, no significant change in mRNA levels was observed for any of the other genes that were examined. Thus, microarray analysis data were quantitatively equivalent to real-time qRT-PCR. By comparing data for wild-type ES cells and EBs, we found that the differentiation of totipotent ES cells into EBs was associated with an increase in mRNA levels of all of the TJ proteins we analysed except for Ybx3 (Table 3C). Thus, in wild-type clones, the mRNA levels increased for claudin-2 (~69.1-fold), claudin-6 (~19.7-fold), claudin-7 (~26.5-fold), occludin (~10.2-fold) and JAM-1 (~8.6-fold), as well as for cingulin (~3.9-fold), ZO-1 (~2.4-fold), ZO-2 (~2.8-fold), ZO-3 (~2.2-fold), PAR-3 (~2.8-fold) and Lfc (~2.9-fold) (Table 3C).

Because the epithelial cells of the outer layer of cystic EBs correspond to visceral endoderm (Doetschman et al., 1985), we determined by microarray analysis the mRNA levels of some genes involved in the transcriptional cascade that controls the differentiation of this embryonic layer (Morrisey et al., 1998). As shown in Table 4, mRNA levels for the transcription factors GATA-6, GATA-4 and HNF-4α, and some of their known

**Table 2. Homozygous (–/–) cingulin-mutant EBs feature selective changes in the expression of some TJ genes**

| Gene | GenBank accession number | Change* (–/– vs +/+) |
|---|---|---|
| Cingulin | P59242 | ND |
| ZO-1 | NM_009386 | NC |
| ZO-2 | NM_011597 | NC |
| ZO-3 | NM_013769 | NC |
| Claudin-2 | BC015252 | 21-fold increase |
| Claudin-6 | BC005718 | 2.4-fold increase |
| Claudin-7 | BC008104 | 3.0-fold increase |
| Occludin | NM_008756 | 2.8-fold increase |
| JAM-1 | BC021876 | NC |
| PAR-3 | NM_033620 | NC |
| Lfc | U28495 | NC |

*$P<0.05$; NC, no change ($P>0.05$); ND, not detected.

**Table 3. Real-time qRT-PCR on wild-type (+/+), heterozygous (+/–) and homozygous (–/–) clones**

| | A: ES cells | | | | B: EBs | | | | C: Differentiation of wild-type ES cells into EBs | |
|---|---|---|---|---|---|---|---|---|---|---|
| | +/– vs +/+ | | –/– vs +/+ | | +/– vs +/+ | | –/– vs +/+ | | | |
| Gene | ΔΔ*Ct* | Fold change* | ΔΔ*Ct* | Fold change* | ΔΔ*Ct* | Fold change* | ΔΔ*Ct* | Fold change* | ΔΔ*Ct* | Fold change* |
| Cingulin | 0.92±0.32 | ↓ 1.9 | ND | ↓ Total | –0.30±0.26 | NC | ND | ↓ Total | –1.97±0.32 | ↑ 3.9 |
| ZO-1 $\alpha^-$ | 0.43±0.10 | NC | 0.22±0.11 | NC | –0.38±0.19 | NC | –0.33±0.21 | NC | –1.25±0.19 | ↑ 2.4 |
| ZO-1 $\alpha^+$ | 0.31±0.14 | NC | 0.16±0.12 | NC | –0.28±0.11 | NC | –0.18±0.13 | NC | –1.27±0.11 | ↑ 2.4 |
| ZO-2 | 0.35±0.15 | NC | 0.25±0.15 | NC | –0.08±0.12 | NC | –0.03±0.15 | NC | –1.47±0.12 | ↑ 2.8 |
| ZO-3 | –0.35±0.32 | NC | –0.42±0.25 | NC | –0.35±0.17 | NC | –0.20±0.14 | NC | –1.13±0.25 | ↑ 2.2 |
| Claudin-2 | –0.16±0.22 | NC | 0.22±0.25 | NC | –3.94±0.41 | ↑ 15.3 | –4.28±0.36 | ↑ 19.4 | –6.11±0.26 | ↑ 69.1 |
| Claudin-6 | –0.33±0.23 | NC | –0.33±0.30 | NC | –1.35±0.14 | ↑ 2.5 | –1.23±0.16 | ↑ 2.3 | –4.30±0.22 | ↑ 19.7 |
| Claudin-7 | –0.25±0.21 | NC | –0.28±0.22 | NC | –1.98±0.09 | ↑ 3.9 | –1.88±0.22 | ↑ 3.7 | –4.73±0.17 | ↑ 26.5 |
| Occludin | –0.08±0.12 | NC | –0.05±0.12 | NC | –1.62±0.32 | ↑ 3.1 | –1.55±0.25 | ↑ 2.9 | –3.35±0.18 | ↑ 10.2 |
| JAM-1 | –0.05±0.06 | NC | 0.07±0.13 | NC | –0.25±0.20 | NC | –0.48±0.25 | NC | –3.10±0.14 | ↑ 8.6 |
| PAR-3 | 0.07±0.15 | NC | 0.00±0.17 | NC | –0.43±0.20 | NC | –0.15±0.14 | NC | –1.50±0.21 | ↑ 2.8 |
| Lfc | 0.09±0.12 | NC | 0.07±0.13 | NC | 0.08±0.22 | NC | –0.22±0.19 | NC | –1.53±0.20 | ↑ 2.9 |
| Ybx3 | –0.13±0.12 | NC | –0.15±0.09 | NC | 0.30±0.15 | NC | 0.22±0.10 | NC | –0.18±0.08 | NC |

*$P<0.05$; NC, no change ($P>0.05$); ND, not detected; arrows indicate up- or downregulation of gene expression.

downstream targets (α-fetoprotein, transferrin, ApoAI and ApoAIV) were significantly increased above wild-type values in cingulin homozygous (–/–) EBs.

### Wild-type and cingulin-mutant epithelial cells form structurally normal TJs within EBs

Wild-type and cingulin-mutant ES cells formed colonies and EBs that appeared similar with regard to growth rate, size and light microscopy morphology (data not shown). Transmission and freeze-fracture electron microscopy were used to assess TJ ultrastructure in cystic EBs. Transmission electron microscopy showed that cystic EBs were lined by an outer layer of visceral endoderm epithelial cells, characterized by apical microvilli projecting into the external medium (Fig. 3A). Occasionally, an inner layer consisting of flattened cells was detected below the epithelial cells (Fig. 3A). No TJs were detected by transmission electron microscopy in this layer.

Transmission and freeze-fracture electron microscopy showed typical TJs in the apical regions of the outer layer of epithelial cells (visceral endoderm) in wild-type (Fig. 3B, Fig. 4B,E), heterozygous (+/–) (Fig. 3C, Fig. 4C,F) and homozygous (–/–) (Fig. 3D, Fig. 4D,G) cystic EBs. Irrespective of the genotype, TJs were organized both as continuous belts, comprising three to five parallel strands spanning long portions of the cell membrane and interlinked by few fibrils (Fig. 4A-D), and as focal arrays, comprising intermingled fibrils that delineated small membrane domains (Fig. 4A,E-G). Quantitative analysis failed to show major differences between the thickness of TJ complexes (typically 0.4-0.6 μm), the number of strands per belt (typically three to five) or the individual fibril length in both focal arrays and belts (typically 0.4-0.5 μm) (Table 5).

### Cingulin mutation alters neither the junctional localization of ZO-1, occludin and claudin-6 nor the permeability of TJs in cystic EBs

To determine the subcellular distribution of TJ proteins, frozen sections of EBs of each of the six clones were immunofluorescently labeled. Of the available antibodies, only those against cingulin, ZO-1, occludin and claudin-6 resulted in specific junctional labeling of the outer layer (visceral endoderm) of epithelial cells lining the cavities of cystic EBs (Fig. 5A-C). No junctional labeling was observed either in other regions of cystic EBs or in non-cystic EBs.

**Table 4. Homozygous (–/–) cingulin-mutant EBs show changes in the expression of some genes involved in visceral endoderm differentiation**

| Gene | GenBank accession number | Fold increase* (–/– vs +/+) |
|---|---|---|
| HNF-4α | NM_008261 | 2.5 |
| GATA-6 | AF179425 | 2.3 |
| GATA-4 | AB075549 | 2.5 |
| α-Fetoprotein | NM_007423 | 42.2 |
| Transferrin | AF440692 | 16.1 |
| ApoAI | NM_009692 | 35.6 |
| ApoAIV | BC010769 | 26.4 |

*$P<0.05$.

Labeling for cingulin (Fig. 5A,B, green channel) was detected in all wild-type (+/+) and heterozygous (+/–) EBs at areas of contact between adjacent cells of the epithelial layer lining the cavities of cystic EBs. As shown by merged images, cingulin was precisely co-localized with ZO-1 (Fig. 5A, red channel) and occludin labeling (Fig. 5B, red channel). The intensities of occludin and ZO-1 labeling were similar in wild-type and mutant EBs, despite the observation that protein levels were altered in mutant EBs by immunoblot analysis (Fig. 2). Labeling of EB sections with anti-claudin-6 antibodies revealed co-localization with ZO-1 at areas of cell-cell contact, and no obvious changes in fluorescent label intensity were observed between wild-type and mutant EBs (Fig. 5C). In homozygous (–/–) EBs, no cingulin labeling was detected at the cell border (Fig. 5A,B, –/–), whereas ZO-1, occludin and claudin-6 labeling were indistinguishable from those of wild-type EBs. Despite the observation that a truncated form of cingulin is detectable by immunoblotting in the Triton-soluble fraction of heterozygous (+/–) and homozygous (–/–) EBs (Fig. 2), we could not unambiguously detect cytoplasmic labeling above background in the heterozygous (+/–) and homozygous (–/–) EBs (Fig. 5A,B, –/–).

To evaluate the permeability of TJs in cystic EBs, we used the covalent cross-linker NHS-LC-Biotin, which binds to proteins on accessible cell surfaces (Chen et al., 1997). EBs from wild-type, heterozygous (+/–) and homozygous (–/–) ES clones showed biotin labeling only on apical surfaces (Fig. 5D), indicating that functional TJs, impermeable to the compound, exist in all these EBs. Labeling of actin filaments with TRITC-phalloidin was intense on the apical membrane and along cell-cell borders, and was similar in wild-type and mutant EBs (Fig. 5D).

## Discussion

The objective of the present study was to determine whether lack of junctional cingulin affects TJ organization and what are the functional consequences of a targeted deletion of the cingulin head domain in epithelial cells. The results demonstrate that lack of junctional cingulin does not prevent TJ formation, and that EBs lacking full-length cingulin and expressing a truncated form of cingulin display altered levels of some TJ proteins and altered expression of TJ-related genes and genes involved in endodermal differentiation.

The cingulin sequence that was deleted by homologous recombination has a crucial role in the junctional recruitment of cingulin and its interactions with other proteins (D'Atri et al., 2002). No full-length cingulin was expressed in homozygous (–/–) EBs, and a truncated form of cingulin was detected in heterozygous (+/–) and homozygous (–/–) EBs. Immunofluorescence analysis revealed no junctional localization of cingulin in homozygous (–/–) epithelial cells, confirming that the truncated protein is not recruited to junctions, in agreement with previous observations (Cordenonsi et al., 1999a; D'Atri et al., 2002). Furthermore, only full-length cingulin was detectable in the Triton-insoluble fraction of EBs, providing biochemical evidence that the truncated protein is cytoplasmic. Our inability to detect specific cytoplasmic labeling in epithelial cells of heterozygous (+/–) and homozygous (–/–) EBs could be due to some loss of the protein upon cell permeabilization and the difficulty in

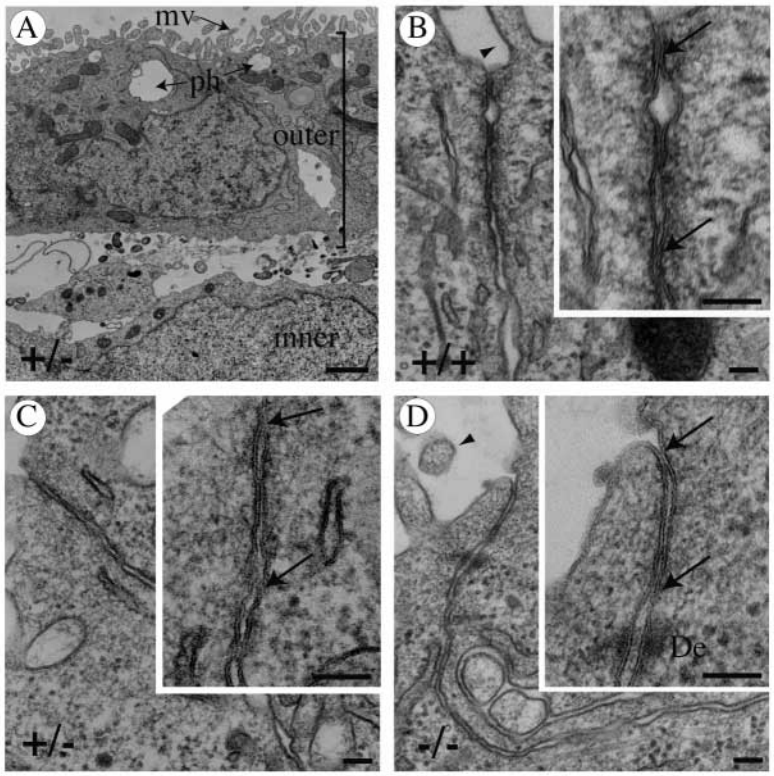


**Fig. 3.** Transmission electron microscopy reveals TJs in wild-type and mutant cystic EBs. Micrographs show junctional complexes between epithelial cells of wild-type (B), heterozygous (+/–) (A,C) and homozygous (–/–) (D) EBs. Images were obtained from cystic EBs sectioned through their centers in a near-equatorial position. The outer surface of the cyst is at the top of each frame. (A) Low-magnification micrograph showing an example of a cystic EB (+/–), comprising an outer layer of epithelial cells (corresponding to visceral endoderm, indicated by bracket) and an inner layer. The outer layer cells were polarized, with apical microvilli (mv) projecting towards the outer surface and phagocytic vesicles (ph) in the cytoplasm. The two layers were usually separated by an intercellular space and the inner layer was not consistently detected. The inner layer of cells is referred to in the literature as ectoderm (Doetschman et al., 1985; Ikeda et al., 1999; Saitou et al., 1998) or undifferentiated cells (Soudais et al., 1995). The same ultrastructure was observed in all wild-type and mutant EBs. (B-D) Higher-magnification micrographs showing the apico-lateral membranes of adjoining outer epithelial cells. Inserts show, at higher magnifications, the areas of junctional complexes. The typical morphology of TJs, with intimate membrane interconnections, is seen irrespective of the cells genotype (B-D, arrows). TJs are occasionally associated with desmosomes (De in D). Scale bars, 2 μm (A), 100 nm (B-D).

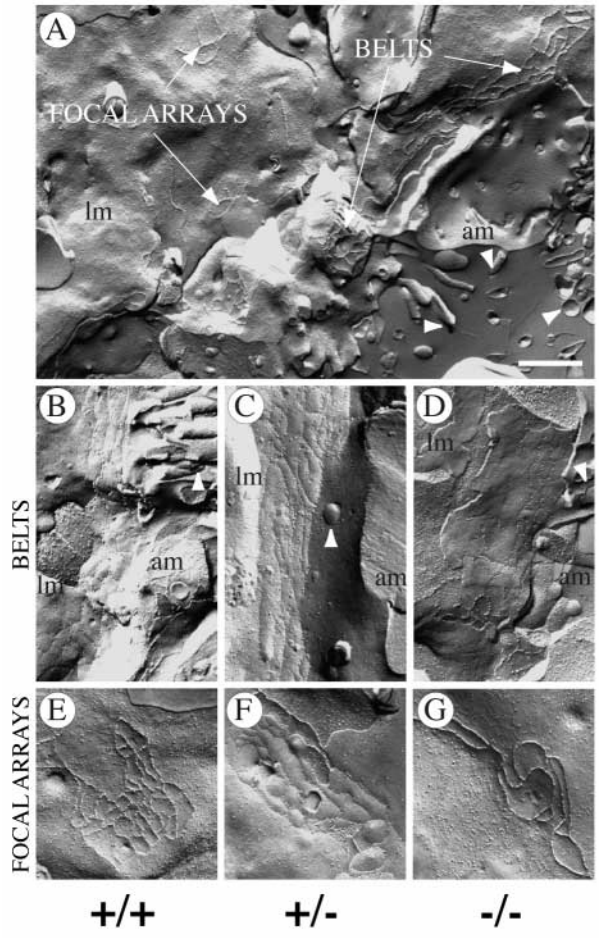


detecting low levels of a diffusely localized protein in confocal optical sections.

TJs with similar morphology were detected by transmission and freeze-fracture electron microscopy between epithelial cells of wild-type (+/+), heterozygous (+/–) and homozygous (–/–) EBs. The TJ barrier function also appeared to be unaffected by the cingulin mutation. The junctional distribution of ZO-1, occludin and claudin-6 in mutant cells was indistinguishable from that seen in wild-type cells. Taken together, these results indicate that, although cingulin interacts with ZO-1, occludin and other TJ proteins through its head domain (Cordenonsi et al., 1999a; Cordenonsi et al., 1999b; D'Atri et al., 2002), targeted deletion of this domain does not prevent the recruitment of these interacting proteins into TJs. Because most TJ proteins interact with multiple partners, it is likely that redundant interactions control their junctional

**Fig. 4.** Freeze-fracture electron microscopy reveals assemblies of TJ fibrils in wild-type and mutant cystic EBs. (A) Low-magnification image of large portions of the plasma membrane of a cystic EB. TJ fibrils are seen arranged both as a continuous belt, separating the apical (am) and the basolateral (lm) membrane domains, and as spatially restricted focal arrays within the basolateral membrane. (B-D) Higher magnification views, showing similar TJ belts (three to five strands thick) in one wild-type (WT1) (B), one heterozygous (+/–) (1;166) (C) and one homozygous (–/–) (3;96) (D) EB clone. Similar results were obtained with other clones (Table 5). (E-G) Higher-magnification views, showing focal arrays of TJ fibrils, which segregate microdomains within the basolateral membrane in wild-type (E), heterozygous (+/–) (F) and homozygous (–/–) (G) EBs. The arrowheads point to microvilli. Scale bars, 0.5 μm (A), 225 nm (B-G).

**Table 5. Quantitative analysis of TJ ultrastructure in EBs**

| Genotype | Clone | TEM | FF | | |
|---|---|---|---|---|---|
| | | TJ thickness (μm) | Belt thickness (μm) | Strands per belt | Fibril length (μm) |
| +/+ | WT1 | 0.52±0.14 (*n*=12) | 0.42±0.05 (*n*=27) | 3.0±0.3 (*n*=27) | 0.50±0.05 (*n*=426) |
| | WT2 | 0.58±0.13 (*n*=15) | 0.51±0.06 (*n*=24) | 4.1±0.4 (*n*=24) | 0.46±0.04 (*n*=775) |
| +/– | 1;10 | 0.57±0.15 (*n*=13) | 0.34±0.04 (*n*=21) | 4.0±0.4 (*n*=21) | 0.50±0.07 (*n*=466) |
| | 1;166 | 0.48±0.10 (*n*=16) | 0.47±0.06 (*n*=15) | 5.3±0.5 (*n*=15) | 0.50±0.04 (*n*=565) |
| –/– | 3;4 | 0.46±0.15 (*n*=15) | 0.24±0.03 (*n*=12) | 3.6±0.4 (*n*=12) | 0.42±0.04 (*n*=331) |
| | 3;96 | 0.48±0.20 (*n*=13) | 0.53±0.07 (*n*=12) | 4.2±0.4 (*n*=12) | 0.43±0.06 (*n*=395) |

TEM, transmission electron microscopy; FF, freeze-fracture.

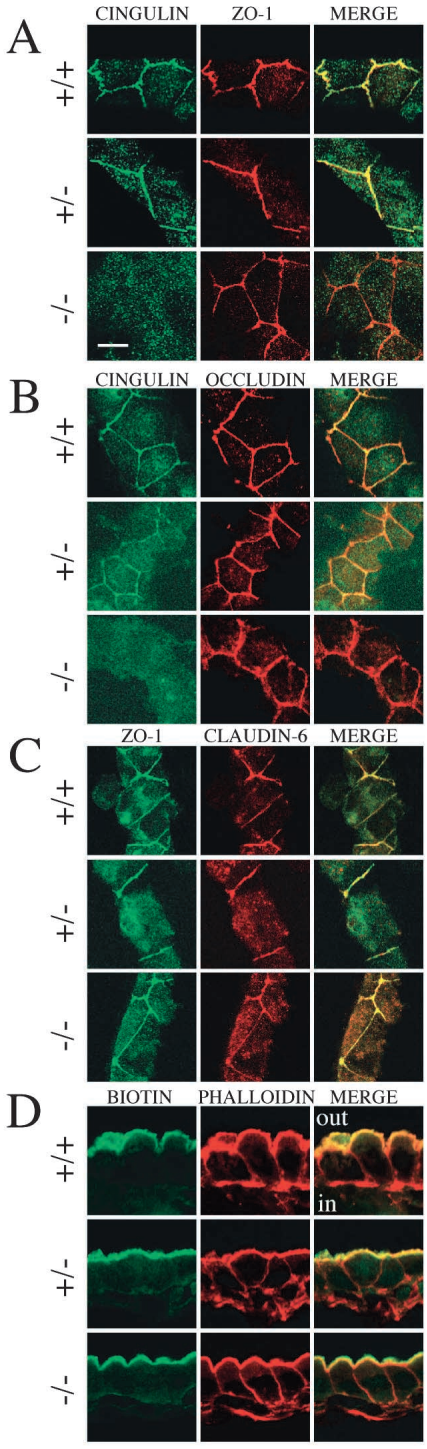


recruitment. For example, ZO-1 forms complexes with ZO-2 and ZO-3 (Balda et al., 1993; Gumbiner et al., 1991; Haskins et al., 1998), and these three proteins interact with occludin, claudins (Fanning et al., 1998; Haskins et al., 1998; Itoh et al., 1999a; Itoh et al., 1999b) and F-actin (Fanning et al., 1998; Itoh et al., 1997; Wittchen et al., 1999). However, ZO-1 recruitment into junctions does not depend on occludin, because ZO-1 is normally localized in occludin-deficient epithelial cells of EBs (Saitou et al., 1998). Although ZO-1 recruitment to TJs appeared to be unaffected by cingulin mutation, its levels were altered in heterozygous and homozygous EBs, supporting the notion of a functionally important interaction (see below). Our data do not exclude the possibility that cingulin-like proteins exist and might compensate for the loss of full-length cingulin in homozygous (–/–) cells, resulting in normal TJs. Consistent with this hypothesis, we recently identified paracingulin (GenBank AAT37906) a protein with significant homology to cingulin, which is junctionally localized when transfected into epithelial cells (S. C. and L.G., unpublished data). Characterization of this protein will provide additional insights into its potential role at TJs.

Lysates of heterozygous (+/–) and homozygous (–/–) EBs contained less ZO-1 and more ZO-2, claudin-6 and occludin proteins than those of wild-type EBs. In addition, Lfc was detected only in homozygous (–/–) EBs. We tested whether these changes in protein levels reflected changes in mRNA

**Fig. 5.** Cingulin mutation does not influence the junctional localization of ZO-1, occludin or claudin-6, or the permeability of TJs to NHS-LC-Biotin in cystic EBs. (A-C) Immunofluorescence analysis of EBs that were fixed, sectioned and stained with antibodies against the antigens indicated above each set of images. Color coding corresponds to secondary antibodies fluorophores used (green, FITC-labeled anti-mouse antibody; red, Cy5-labeled anti-rabbit antibody), except in the case of the double cingulin-ZO-1 labeling, in which color was inverted (rabbit anti-cingulin antibody followed by Cy5-anti-rabbit antibody, and rat anti-ZO-1 antibody followed by FITC-anti-rat antibody were used). Monoclonal antibody against cingulin was used for co-localization with occludin (B). In 'merge' images, the yellow color shows co-localization of proteins. Junctional cingulin labeling is not detected in homozygous (–/–) cystic EBs (A,B). (D) Biotin permeability assay. EBs were incubated in 1 mg $ml^{-1}$ NHS-LC-Biotin, washed, fixed, sectioned and stained with FITC-conjugated avidin (green) and TRITC-phalloidin (red) to visualize NHS-LC-Biotin and actin filaments, respectively. Epithelial cells with functional TJs exclude NHS-LC-Biotin from intercellular spaces, resulting in labeling being restricted to apical surfaces. 'Out' and 'In' in the (+/+) merge image indicate spaces outside and inside the cavity of the EBs, respectively. Scale bar, 10 μm.

levels, by measuring mRNA levels by microarray and real-time qRT-PCR analysis. In the case of claudin-6 and occludin, the increase in protein levels was correlated with a significant increase in mRNA levels in both heterozygous (+/–) and homozygous (–/–) EBs. Thus, increased claudin-6 and occludin protein levels reflected changes in transcript levels. However, for occludin, we speculate that additional post-transcriptional mechanisms might be involved, because there was a larger increase in occludin protein levels in heterozygous (+/–) and homozygous (–/–) EBs than for claudin-6, whereas the mRNA increases were similar for the two proteins. Despite the observed increases in protein and transcript levels, the immunofluorescent distribution of occludin and claudin-6 were similar in wild-type and mutant EBs. In addition, electron microscopy revealed similar TJ fibrils and belts, which are made of occludin and claudins (Tsukita et al., 2001), in wild-type and mutant EBs. Thus, altered protein and transcript levels for TJ fibril components did not appear to influence significantly the assembly of TJ strands. Because the levels of mRNAs encoding ZO-1, ZO-2 and Lfc were not significantly different in wild-type and mutant EBs, we speculate that the altered steady-state levels of these TJ proteins were a consequence of decreased (ZO-1) or increased (ZO-2 and Lfc) protein stability, and/or changes in translation efficiency, caused by the mutation of cingulin. Because cingulin interacts in vivo with ZO-1 and ZO-2 (Cordenonsi et al., 1999a; D'Atri et al., 2002), one possible functional scenario is that cingulin mutation induces decreased ZO-1 protein stability, with ZO-2 levels increased as a compensatory mechanism. Furthermore, the increased Lfc levels in homozygous (–/–) EBs indicate a functional link between cingulin and Lfc.

Transcript levels of claudin-2, claudin-6, claudin-7, occludin and several transcription factors (see below) were increased in cingulin-mutant EBs. The increases in claudin-2, claudin-6, claudin-7 and occludin mRNAs were not apparent in ES cells, demonstrating that cingulin mutation affected mRNA levels only in differentiated cells, which contain TJs. To our knowledge, this is the first time that significant changes in transcript levels have been reported following mutation of a structural component of TJs. Although our results suggest that cingulin might be implicated in the regulation of gene expression, previous studies have shown that cytoskeletal and junction-associated proteins such as β-catenin (Behrens et al., 1996), actin (Sotiropoulos et al., 1999) and tubulin (Ziegelbauer et al., 2001) are implicated in transcriptional regulation. In addition, the TJ proteins ZO-1 and ZO-2 have been detected in the nucleus (Gottardi et al., 1996; Islas et al., 2002) and have been shown to interact with the transcription factors ZONAB (Balda and Matter, 2000), Fos, Jun and C/EBP (Betanzos et al., 2004), suggesting that TJ proteins can regulate gene activity by modulating the nuclear accumulation of transcription factors.

What is the mechanism through which cingulin mutation affects mRNA levels of claudin-2, claudin-6, claudin-7 and occludin? The simplest hypothesis is that cingulin directly influences the transcription rate of these TJ genes or the stability of their respective mRNAs. However, although cingulin has been detected in the nucleus (Citi and Cordenonsi, 1999; Nakamura et al., 2000), and exogenously expressed cingulin head domain can localize to the nucleus (D'Atri et al., 2002), nothing is known about its interaction with nucleic acids or its role as a transcription factor. Another hypothesis is that cingulin mutation affects the level of mRNAs coding for TJ proteins indirectly, by perturbing transcriptional and/or translational regulatory networks that control the expression and mRNA stability of TJ-protein genes. Consistent with this possibility, we noticed that the genes whose mRNA levels were increased in cingulin-mutant EBs (claudin-2, claudin-6, claudin-7 and occludin) are the same as those that are induced by retinoic-acid treatment or overexpression of the hepatocyte nuclear receptor HNF-4α in F9 murine embryonal carcinoma cells (Chiba et al., 2003; Kubota et al., 2001). Strikingly, we showed increased transcript levels for the transcription factors HNF-4α, GATA-4 and GATA-6 in homozygous (–/–) EBs. HNF-4α is an early endodermal marker and, together with GATA-4, it acts as a target of GATA-6 (Morrisey et al., 1998). In turn, HNF-4α controls the transcription of late endodermal markers such as α-fetoprotein, transferrin, ApoAI and ApoAIV (Morrisey et al., 1998). Loss of GATA-6, GATA-4 or HNF-4α leads to defects in visceral endoderm differentiation, resulting in cell death within the ectoderm of mouse embryos (Chen et al., 1994; Koutsourakis et al., 1999; Morrisey et al., 1998; Soudais et al., 1995). Because the mRNA levels of all these transcription factors and targets were significantly increased in homozygous (–/–) EBs, our results strongly indicate that the mechanism through which cingulin mutation influences the expression of occludin and claudin genes is by altering the levels of GATA-6, GATA-4 and HNF-4α.

The observation that the phenotype of heterozygous (+/–) EBs was almost identical to that of homozygous (–/–) EBs indicates that the differences observed in protein and transcript levels are due either to haploinsufficiency or to a dominant-negative effect of the truncated cingulin. Cytoplasmic truncated cingulin might influence protein and mRNA levels by one or more of several mechanisms. Truncated cingulin might affect the dynamics of the actin cytoskeleton directly or indirectly (for example, through modulation of the Rho regulator Lfc) and thus change the activity and/or nuclear accumulation of transcription factors that are regulated by the organization of the actin cytoskeleton (Sotiropoulos et al., 1999). Another possibility is that truncated cingulin interacts directly with transcription factors and affects their subcellular distribution. Experiments to test these hypotheses are beyond the scope of the present study and will be carried out in the future.

In summary, we have demonstrated that targeted deletion of most of the head domain of cingulin in ES cells abolishes cingulin junctional recruitment without preventing TJ formation in epithelial cells of differentiated EBs. We showed that junctional cingulin is not required either for junctional targeting of ZO-1, occludin and claudin-6 or for the formation of a paracellular TJ barrier. We showed that, in EBs, cingulin mutation results in altered protein levels for some TJ proteins and in increased transcript levels for claudin-2, claudin-6, claudin-7 and occludin, probably via the activation of the GATA-6/HNF-4α visceral-endoderm differentiation pathway. Although additional studies will be necessary to investigate the pathway linking cingulin and HNF-4α to the expression of claudin and occludin genes, these results suggest for the first time that cingulin might participate in regulating the expression of genes implicated in epithelial differentiation.

We are very grateful to D. Duboule for his generosity in providing us with ES cells and facilities to initiate this work. We are also indebted to M. Friedli and F. Chabaud for assistance in ES cell culture, T. Laroche for help with confocal microscopy, and P. Descombes and O. Schaad for assistance in microarray analysis. We also thank F. Spitz, J. Ripperger, F. Damiola and N. Preitner for advice and reagents, F. Nadalutti for help in targeting vector construction, the colleagues cited in the text for generous gifts of antibodies, and U. Schibler and H. Goodson for stimulating discussions. This study was supported by grants from the Swiss National Fund, the Swiss Cancer League, the State of Geneva, the MIUR, and the NCCR Research Pole 'Frontiers in Genetics'. The Meda team was supported by the Swiss National Fund, the European Union, and the National Institute of Health. LG was supported by a Roche Research Foundation Fellowship.

## References

**Balda, M. S. and Anderson, J. M.** (1993). Two classes of tight junctions are revealed by ZO-1 isoforms. *Am. J. Physiol.* **264**, C918-C924.

**Balda, M. S. and Matter, K.** (2000). The tight junction protein ZO-1 and an interacting transcription factor regulate ErbB-2 expression. *EMBO J.* **19**, 2024-2033.

**Balda, M. S., Gonzalez-Mariscal, L., Matter, K., Cereijdo, M. and Anderson, J. M.** (1993). Assembly of the tight junction: the role of diacylglycerol. *J. Cell Biol.* **123**, 293-302.

**Bazzoni, G., Martinez-Estrada, O. M., Orsenigo, F., Cordenonsi, M., Citi, S. and Dejana, E.** (2000). Interaction of junctional adhesion molecule with the tight junction components ZO-1, cingulin, and occludin. *J. Biol. Chem.* **275**, 20520-20526.

**Behrens, J., von Kries, J. P., Kuhl, M., Bruhn, L., Wedlich, D., Grosschedl, R. and Birchmeier, W.** (1996). Functional interaction of beta-catenin with the transcription factor LEF-1. *Nature* **382**, 638-642.

**Ben-Yosef, T., Belyantseva, I. A., Saunders, T. L., Hughes, E. D., Kawamoto, K., van Itallie, C. M., Beyer, L. A., Halsey, K., Gardner, D. J., Wilcox, E. R. et al.** (2003). Claudin 14 knockout mice, a model for autosomal recessive deafness DFNB29, are deaf due to cochlear hair cell degeneration. *Hum. Mol. Genet.* **12**, 2049-2061.

**Benais-Pont, G., Punn, A., Flores-Maldonado, C., Eckert, J., Raposo, G., Fleming, T. P., Cereijido, M., Balda, M. S. and Matter, K.** (2003). Identification of a tight junction-associated guanine nucleotide exchange factor that activates Rho and regulates paracellular permeability. *J. Cell Biol.* **160**, 729-740.

**Betanzos, A., Huerta, M., Lopez-Bayghen, E., Azuara, E., Amerena, J. and Gonzalez-Mariscal, L.** (2004). The tight junction protein ZO-2 associates with Jun, Fos and C/EBP transcription factors in epithelial cells. *Exp. Cell Res.* **292**, 51-66.

**Cardellini, P., Davanzo, G. and Citi, S.** (1996). Tight junctions in early amphibian development: detection of junctional cingulin from the 2-cell stage and its localization at the boundary of distinct membrane domains in dividing blastomeres in low calcium. *Dev. Dyn.* **207**, 104-113.

**Chen, W. S., Manova, K., Weinstein, D. C., Duncan, S. A., Plump, A. S., Prezioso, V. R., Bachvarova, R. F. and Darnell, J. E., Jr** (1994). Disruption of the *HNF-4* gene, expressed in visceral endoderm, leads to cell death in embryonic ectoderm and impaired gastrulation of mouse embryos. *Genes Dev.* **8**, 2466-2477.

**Chen, Y., Merzdorf, C., Paul, D. L. and Goodenough, D. A.** (1997). COOH terminus of occludin is required for tight junction barrier function in early *Xenopus* embryos. *J. Cell Biol.* **138**, 891-899.

**Chiba, H., Gotoh, T., Kojima, T., Satohisa, S., Kikuchi, K., Osanai, M. and Sawada, N.** (2003). Hepatocyte nuclear factor (HNF)-4alpha triggers formation of functional tight junctions and establishment of polarized epithelial morphology in F9 embryonal carcinoma cells. *Exp. Cell Res.* **286**, 288-297.

**Citi, S.** (2001). The cytoplasmic plaque proteins of tight junctions. In *Tight Junctions*, 2nd edn (ed. M. Cereijido and J. Anderson), pp. 231-264. Boca Raton, FL: CRC Press.

**Citi, S. and Cordenonsi, M.** (1999). The molecular basis for the structure, function and regulation of tight junctions. In *Adhesive Interactions of Cells*, Vol. 28 (ed. D. R. Garrod, A. J. North and M. A. J. Chidgey), pp. 203-233. Greenwich, CT: JAI Press.

**Citi, S., Sabanay, H., Jakes, R., Geiger, B. and Kendrick-Jones, J.** (1988). Cingulin, a new peripheral component of tight junctions. *Nature* **333**, 272-276.

**Citi, S., D'Atri, F. and Parry, D. A. D.** (2000). Human and *Xenopus* cingulin share a modular organization of the coiled-coil rod domain: predictions for intra- and intermolecular assembly. *J. Struct. Biol.* **131**, 135-145.

**Cordenonsi, M., D'Atri, F., Hammar, E., Parry, D. A., Kendrick-Jones, J., Shore, D. and Citi, S.** (1999a). Cingulin contains globular and coiled-coil domains and interacts with ZO-1, ZO-2, ZO-3, and myosin. *J. Cell Biol.* **147**, 1569-1582.

**Cordenonsi, M., Turco, F., D'Atri, F., Hammar, E., Martinucci, G., Meggio, F. and Citi, S.** (1999b). *Xenopus laevis* occludin: identification of in vitro phosphorylation sites by protein kinase CK2 and association with cingulin. *Eur. J. Biochem.* **264**, 374-384.

**D'Atri, F. and Citi, S.** (2001). Cingulin interacts with F-actin in vitro. *FEBS Lett.* **507**, 21-24.

**D'Atri, F. and Citi, S.** (2002). Molecular complexity of vertebrate tight junctions. *Mol. Membr. Biol.* **19**, 103-112.

**D'Atri, F., Nadalutti, F. and Citi, S.** (2002). Evidence for a functional interaction between cingulin and ZO-1 in cultured cells. *J. Biol. Chem.* **277**, 27757-27764.

**Doetschman, T. C., Eistetter, H., Katz, M., Schmidt, W. and Kemler, R.** (1985). The in vitro development of blastocyst-derived embryonic stem cell lines: formation of visceral yolk sac, blood islands and myocardium. *J. Embryol. Exp. Morphol.* **87**, 27-45.

**Ebnet, K., Schulz, C. U., Meyer Zu Brickwedde, M. K., Pendl, G. G. and Vestweber, D.** (2000). Junctional Adhesion Molecule (JAM) interacts with the PDZ domain containing proteins AF-6 and ZO-1. *J. Biol. Chem.* **275**, 27979-27988.

**Fanning, A. S., Jameson, B. J., Jesaitis, L. A. and Anderson, J. M.** (1998). The tight junction protein ZO-1 establishes a link between the transmembrane protein occludin and the actin cytoskeleton. *J. Biol. Chem.* **273**, 29745-29753.

**Fesenko, I., Kurth, T., Sheth, B., Fleming, T. P., Citi, S. and Hausen, P.** (2000). Tight junction biogenesis in the early *Xenopus* embryo. *Mech. Dev.* **96**, 51-65.

**Fleming, T. P., Hay, M., Javed, Q. and Citi, S.** (1993). Localisation of tight junction protein cingulin is temporally and spatially regulated during early mouse development. *Development* **117**, 1135-1144.

**Furuse, M., Hata, M., Furuse, K., Yoshida, Y., Haratake, A., Sugitani, Y., Noda, T., Kubo, A. and Tsukita, S.** (2002). Claudin-based tight junctions are crucial for the mammalian epidermal barrier: a lesson from claudin-1-deficient mice. *J. Cell Biol.* **156**, 1099-1111.

**Gonzalez-Mariscal, L., Betanzos, A., Nava, P. and Jaramillo, B. E.** (2003). Tight junction proteins. *Prog. Biophys. Mol. Biol.* **81**, 1-44.

**Gottardi, C. J., Arpin, M., Fanning, A. S. and Louvard, D.** (1996). The junction-associated protein, zonula occludens-1, localizes to the nucleus before the maturation and during the remodeling of cell-cell contacts. *Proc. Natl. Acad. Sci. USA* **93**, 10779-10784.

**Gow, A., Southwood, C. M., Li, J. S., Pariali, M., Riordan, G. P., Brodie, S. E., Danias, J., Bronstein, J. M., Kachar, B. and Lazzarini, R. A.** (1999). CNS myelin and Sertoli cell tight junction strands are absent in Osp/claudin-11 null mice. *Cell* **99**, 649-659.

**Gumbiner, B., Lowenkopf, T. and Apatira, D.** (1991). Identification of a 160 kDa polypeptide that binds to the tight junction protein ZO-1. *Proc. Natl. Acad. Sci. USA* **88**, 3460-3464.

**Haskins, J., Gu, L., Wittchen, E. S., Hibbard, J. and Stevenson, B. R.** (1998). ZO-3, a novel member of the MAGUK protein family found at the tight junction, interacts with ZO-1 and occludin. *J. Cell Biol.* **141**, 199-208.

**Hirano, T., Kobayashi, N., Itoh, T., Takasuga, A., Nakamaru, T., Hirotsune, S. and Sugimoto, Y.** (2000). Null mutation of PCLN-1/Claudin-16 results in bovine chronic interstitial nephritis. *Genome Res.* **10**, 659-663.

**Ikeda, W., Nakanishi, H., Miyoshi, J., Mandai, K., Ishizaki, H., Tanaka, M., Togawa, A., Takahashi, K., Nishioka, H., Yoshida, H. et al.** (1999). Afadin: a key molecule essential for structural organization of cell-cell junctions of polarized epithelia during embryogenesis. *J. Cell Biol.* **146**, 1117-1132.

**Islas, S., Vega, J., Ponce, L. and Gonzalez-Mariscal, L.** (2002). Nuclear localization of the tight junction protein ZO-2 in epithelial cells. *Exp. Cell Res.* **274**, 138-148.

**Itoh, M., Nagafuchi, A., Moroi, S. and Tsukita, S.** (1997). Involvement of ZO-1 in cadherin-based cell adhesion through its direct binding to alpha catenin and actin filaments. *J. Cell Biol.* **138**, 181-192.

**Itoh, M., Furuse, M., Morita, K., Kubota, K., Saitou, M. and Tsukita, S.** (1999a). Direct binding of three tight junction-associated MAGUKs, ZO-1,

ZO-2, and ZO-3, with the COOH termini of claudins. *J. Cell Biol.* **147**, 1351-1363.

**Itoh, M., Morita, K. and Tsukita, S.** (1999b). Characterization of ZO-2 as a MAGUK family member associated with tight as well as adherens junctions with a binding affinity to occludin and alpha catenin. *J. Biol. Chem.* **274**, 5981-5986.

**Izumi, Y., Hirose, T., Tamai, Y., Hirai, S., Nagashima, Y., Fujimoto, T., Tabuse, Y., Kemphues, K. J. and Ohno, S.** (1998). An atypical PKC directly associates and colocalizes at the epithelial tight junction with ASIP, a mammalian homologue of *Caenorhabditis elegans* polarity protein PAR-3. *J. Cell Biol.* **143**, 95-106.

**Koutsourakis, M., Langeveld, A., Patient, R., Beddington, R. and Grosveld, F.** (1999). The transcription factor GATA6 is essential for early extraembryonic development. *Development* **126**, 723-732.

**Kubota, H., Chiba, H., Takakuwa, Y., Osanai, M., Tobioka, H., Kohama, G., Mori, M. and Sawada, N.** (2001). Retinoid X receptor alpha and retinoic acid receptor gamma mediate expression of genes encoding tight-junction proteins and barrier function in F9 cells during visceral endodermal differentiation. *Exp. Cell Res.* **263**, 163-172.

**Martin-Padura, I., Lostaglio, S., Schneemann, M., Williams, L., Romano, M., Fruscella, P., Panzeri, C., Stoppacciaro, A., Ruco, L., Villa, A. et al.** (1998). Junctional adhesion molecule, a novel member of the immunoglobulin superfamily that distributes at intercellular junctions and modulates monocyte transmigration. *J. Cell Biol.* **142**, 117-127.

**Matter, K. and Balda, M. S.** (2003). Signalling to and from tight junctions. *Nat. Rev. Mol. Cell Biol.* **4**, 225-237.

**Morita, K., Sasaki, H., Furuse, M. and Tsukita, S.** (1999). Endothelial claudin: claudin-5/TMVCF constitutes tight junction strands in endothelial cells. *J. Cell Biol.* **147**, 185-194.

**Morrisey, E. E., Tang, Z., Sigrist, K., Lu, M. M., Jiang, F., Ip, H. S. and Parmacek, M. S.** (1998). GATA6 regulates HNF4 and is required for differentiation of visceral endoderm in the mouse embryo. *Genes Dev.* **12**, 3579-3590.

**Nakamura, T., Blechman, J., Tada, S., Rozovskaia, T., Itoyama, T., Bullrich, F., Mazo, A., Croce, C. M., Geiger, B. and Canaani, E.** (2000). huASH1 protein, a putative transcription factor encoded by a human homologue of the *Drosophila ash1* gene, localizes to both nuclei and cell-cell tight junctions. *Proc. Natl. Acad. Sci. USA* **97**, 7284-7289.

**Nitta, T., Hata, M., Gotoh, S., Seo, Y., Sasaki, H., Hashimoto, N., Furuse, M. and Tsukita, S.** (2003). Size-selective loosening of the blood-brain barrier in claudin-5-deficient mice. *J. Cell Biol.* **161**, 653-660.

**Saitou, M., Fujimoto, K., Doi, Y., Itoh, M., Fujimoto, T., Furuse, M., Takano, H., Noda, T. and Tsukita, S.** (1998). Occludin-deficient embryonic stem cells can differentiate into polarized epithelial cells bearing tight junctions. *J. Cell Biol.* **141**, 397-408.

**Saitou, M., Furuse, M., Sasaki, H., Schulzke, J. D., Fromm, M., Takano, H., Noda, T. and Tsukita, S.** (2000). Complex phenotype of mice lacking occludin, a component of tight junction strands. *Mol. Biol. Cell* **11**, 4131-4142.

**Sheth, B., Fesenko, I., Collins, J. E., Moran, B., Wild, A. E., Anderson, J. M. and Fleming, T. P.** (1997). Tight junction assembly during mouse blastocyst formation is regulated by late expression of ZO-1 alpha$^{+}$ isoform. *Development* **124**, 2027-2037.

**Simon, D. B., Lu, Y., Choate, K. A., Velazquez, H., Al-Sabban, E., Praga, M., Casari, G., Bettinelli, A., Colussi, G., Rodriguez-Soriano, J. et al.** (1999). Paracellin-1, a renal tight junction protein required for paracellular $Mg^{2+}$ resorption. *Science* **285**, 103-106.

**Sotiropoulos, A., Gineitis, D., Copeland, J. and Treisman, R.** (1999). Signal-regulated activation of serum response factor is mediated by changes in actin dynamics. *Cell* **98**, 159-169.

**Soudais, C., Bielinska, M., Heikinheimo, M., MacArthur, C. A., Narita, N., Saffitz, J. E., Simon, M. C., Leiden, J. M. and Wilson, D. B.** (1995). Targeted mutagenesis of the transcription factor GATA-4 gene in mouse embryonic stem cells disrupts visceral endoderm differentiation in vitro. *Development* **121**, 3877-3888.

**Stevenson, B. R., Siliciano, J. D., Mooseker, M. S. and Goodenough, D. A.** (1986). Identification of ZO-1: a high molecular weight polypeptide associated with the tight junction (zonula occludens) in a variety of epithelia. *J. Cell Biol.* **103**, 755-766.

**Tsukita, S., Furuse, M. and Itoh, M.** (2001). Multifunctional strands in tight junctions. *Nat. Rev. Mol. Cell Biol.* **2**, 285-293.

**Wilcox, E. R., Burton, Q. L., Naz, S., Riazuddin, S., Smith, T. N., Ploplis, B., Belyantseva, I., Ben-Yosef, T., Liburd, N. A., Morell, R. J. et al.** (2001). Mutations in the gene encoding tight junction claudin-14 cause autosomal recessive deafness DFNB29. *Cell* **104**, 165-172.

**Willott, E., Balda, M. S., Heintzelman, M., Jameson, B. and Anderson, J. M.** (1992). Localization and differential expression of two isoforms of the tight junction protein ZO-1. *Am. J. Physiol.* **262**, C1119-C1124.

**Wittchen, E. S., Haskins, J. and Stevenson, B. R.** (1999). Protein interactions at the tight junction. Actin has multiple binding partners, and ZO-1 forms independent complexes with ZO-2 and ZO-3. *J. Biol. Chem.* **274**, 35179-35185.

**Zhadanov, A. B., Provance, D. W., Speer, C. A., Coffin, J. D., Goss, D., Blixt, J. A., Reichert, C. M. and Mercer, J. A.** (1999). Absence of the tight junctional protein AF-6 disrupts epithelial cell-cell junctions and cell polarity during mouse development. *Curr. Biol.* **9**, 880-888.

**Ziegelbauer, J., Shan, B., Yager, D., Larabell, C., Hoffmann, B. and Tjian, R.** (2001). Transcription factor MIZ-1 is regulated via microtubule association. *Mol. Cell* **8**, 339-349.